Environmental Science Nano

ROYAL SOCIETY OF CHEMISTRY

PAPER

View Article Online
View Journal

Cite this: DOI: 10.1039/d4en00014e

Overlooked impact of surface hydroxylation on the solubility of less-soluble compounds: a case study of CeO_2†

Tatiana V. Plakhova, [a] Anna Yu. Romanchuk, [a] Anastasia D. Konyukhova,[a] Irina F. Seregina,[a] Alexander E. Baranchikov, [b] Roman D. Svetogorov, [ac] Maxwell W. Terban, [d] Vladimir K. Ivanov [be] and Stepan N. Kalmykov *[a]

Received 5th January 2024,
Accepted 21st June 2024

DOI: 10.1039/d4en00014e

rsc.li/es-nano

Unexpectedly, the solubility of CeO_2 nanoparticles (NPs) at 25 °C does not depend on particle size, but is significantly affected by the sample's thermal pre-treatment. The classical interpretation of NPs' solubility proposed by the Gibbs–Thompson or Kelvin equations fails to describe the experimental data on CeO_2 solubility obtained in this study. Thermal treatment did not change the samples' morphological characteristics, while slightly affecting NP hydroxylation and local crystallinity. The differences in the solubility of dried and non-treated CeO_2 particles were most noticeable at pH < 4, and dissolved cerium concentration was much lower in the case of the dried sample. After prolonged storage (up to 4.5 years) of CeO_2 NPs in aqueous media, the solubility of dried samples gradually increased, while for non-treated samples it remained unchanged. Based on the example of CeO_2, the dissolution laws of other less soluble nanomaterials should be reconsidered.

Environmental significance

In view of the high demand for CeO_2-based materials, understanding their dissolution behaviour is imperative. Ceria nanoparticles, whether freshly made and fully hydroxylated or dried, may exhibit distinct environmental behaviours, as surface hydroxylation is crucial in determining their catalytic and biological properties. Unexpectedly, hydroxylated CeO_2 nanoparticles exhibit greater long-term stability than dried ones which significantly advances our understanding of nanoscale materials' dynamics in environmental science. Analogies between cerium dioxide and actinide dioxides are vital for environmental considerations, emphasising the necessity of comprehending the influence of water on the long-term behaviour of these materials and the potential spread of radionuclides through groundwater systems.

Introduction

Rapid advances in nanoscience and nanotechnology, in the 21st century, have created a growing demand for nanomaterials possessing unique properties for various fields of application, from catalysts and accumulators to pharmaceuticals. A decrease in particle size to a few nanometres leads to a significant increase in surface-to-volume ratio and the emergence of unusual effects responsible for size-specific properties, *e.g.*, optical, magnetic and catalytic.[1–4] Mass production of nanomaterials inevitably results in their release into the environment. The impact of engineered nanoparticles (NPs) on biosystems remains debatable and is probably strongly related to their physicochemical properties.[5–7] Living organisms can easily absorb NPs through ingestion, respiration, or both, increasing NPs' exposure to the ecosystem.[8] In addition, various analytical techniques have revealed that a very large number of NPs could exist in the environment as a result of natural NP production.[9] NPs can be dissolved in biological media, leading to the release of toxic metal ions.[10] Thus, the dissolution of natural and engineered NPs can have significant consequences for ecotoxicity.

[a] *Lomonosov Moscow State University, Department of Chemistry, Leninskie Gory 1/3, 119991 Moscow, Russia. E-mail: stepan@radio.chem.msu.ru*
[b] *Kurnakov Institute of General and Inorganic Chemistry of the Russian Academy of Sciences, Leninskii prosp. 31, 117901 Moscow, Russia*
[c] *National Research Centre "Kurchatov Institute", Akademika Kurchatova pl. 1, 123182 Moscow, Russia*
[d] *Max Planck Institute for Solid State Research, Heisenbergstraße 1, 70569 Stuttgart, Germany*
[e] *National Research University Higher School of Economics, Myasnitskaya st. 20, 101000 Moscow, Russia*

† Electronic supplementary information (ESI) available: HRTEM images and ED data; XRD data; Ce L_3 edge HERFD-XAS spectra; PDF G(r) experimental data and fit results; refined parameter values; dissolution curves; dissolution rate constants; comparison of different centrifugation. See DOI: **https://doi.org/10.1039/d4en00014e**

A relevant factor to the issue of NPs in the environment is that they might be thermodynamically unstable and tend to reduce surface energy by coarsening *via* dissolution/precipitation processes.[11] Nevertheless, recent advances in measuring the surface enthalpy of metal oxide materials[12] indicate that some solids could be thermodynamically stable as NPs, under certain conditions.[13–17] For example, Navrotsky *et al.*[18] showed size-related thermodynamic differences among iron oxide phases. A lower surface enthalpy allows oxyhydroxides to exist with larger surface areas, and to be more thermodynamically stable than anhydrous oxides. Along with the possible coarsening of particles, this phenomenon must be taken into account when predicting NPs' spread in the environment. This is especially important for the environmental concerns over the radioactive nanoparticles. The insights in the interaction of actinide oxides with aqueous media must be taken into consideration when regarding nuclear fuel storage or disposal.[19]

Cerium dioxide (CeO_2, ceria) is a multifunctional material that has great promise for many technological applications, including catalysts, sensors, biomaterials, *etc.*[20–24] Based on theoretical predictions, CeO_2 is considered to be very poorly soluble in water.[25] Thus, it could be a suitable model for understanding the processes occurring with other less soluble functional materials in the environment. At the same time, experimental data on CeO_2 behaviour in aqueous media are fragmentary. There are virtually no empirical thermodynamic or kinetic constants (the solubility product value, dissolution rate constants, *etc.*) that can adequately model or predict CeO_2 solubility. The dissolution of CeO_2 and other inorganic materials is strongly influenced by particle size, the composition of the aqueous media, the pH value and reduction potential. A solubility study of 5 nm CeO_2 NPs at 0.01 M ionic strength has been reported earlier, with a reductive dissolution model proposed for data interpretation.[26] There have also been several studies where CeO_2 NP dissolution has been investigated in media of biological and environmental significance.[27–30] Some recent studies have demonstrated a dependence of CeO_2 solubility on the particle size.[27,31,32] However, it is worth noting that in these studies, the presence of anionic phosphate species in the solution could trigger the formation of cerium phosphate phases, subsequently affecting the overall solubility.

The present study investigated the solubility of CeO_2 NPs and associated processes (dissolution and phase transformation) in aqueous media with low ionic strength, to provide deeper insights into the size effect and the specific impact of the hydroxylated oxide surface, and to establish a solubility product. The present work also evaluated short-term and long-term CeO_2 behaviour in solutions at different pH values, and a careful assessment of the effects of NPs' size, thermal treatment and other subtle factors on CeO_2 solubility was made. The data obtained provide some unexpected information on the dissolution trends of less soluble substances.

Experimental

CeO_2 NP synthesis procedure

Aqueous stock solutions of $Ce(NO_3)_3{\cdot}6H_2O$ (Sigma Aldrich) of 0.001 M and 0.8 M concentrations were prepared using MilliQ water. For CeO_2 NP precipitation, the stock solutions were added to a five-fold volume excess of 3 M aqueous ammonia, under continuous stirring at room temperature. Yellow precipitates were formed, which were separated by centrifugation and washed three times with MilliQ water to remove soluble admixtures. For further characterisation, CeO_2 samples were prepared in three different ways. Hereafter, non-treated samples refer to as-prepared CeO_2 NPs after the synthesis procedure without any further treatment; samples dried at 40 °C refer to as-prepared CeO_2 NPs after drying overnight in an ambient environment at 40 °C; samples dried at 150 °C refer to as-prepared CeO_2 NPs after drying overnight in an ambient environment at 150 °C. In addition to conventional drying approaches, the freeze-drying method was used (LS-1000 lyophilic dryer). The as-prepared CeO_2 precipitate was frozen at −52 °C and dried at a pressure of 0.32 mm Hg; the temperature during the drying process did not exceed 0 °C.

Solubility study

The NPs' solubility was studied using the undersaturation method. A small amount of CeO_2 NPs (non-treated, dried at 40 °C or dried at 150 °C) in the form of concentrated aqueous suspension was put into polypropylene tubes. Overall cerium concentration in CeO_2 NP suspensions was 0.01 M. pH values were fixed in the range of 1.5–6 by the successive addition of dilute solutions of NaOH and $HClO_4$. The pH values of the resulting suspensions were determined using an InLab Expert Pro pH electrode (Mettler Toledo). Solubility studies were performed at a constant ionic strength (0.01 M $NaClO_4$). CeO_2 NP suspensions were stored in a laboratory thermostat at 25.0 ± 0.5 °C.

To analyse the concentration of dissolved cerium, the liquid phase was separated from the CeO_2 NPs by centrifugation using a Beckman Coulter Allegra 64R centrifuge. The duration and speed of centrifugation for the complete separation of the solid phase were calculated from the rotor parameters, for each sample individually. To verify the separation efficiency of the solid phase, ultrafiltration (Millipore filter, 3 kDa) and ultracentrifugation (Beckman Optima TLX Ultracentrifuge, TLA-110 rotor) were used. Aliquots of the samples were analysed as a function of the pH value or equilibration time ranging from a few days to a few years. Cerium concentration in the samples was measured by inductively coupled plasma mass spectrometry (ICP-MS) on an Agilent 7500C inductively coupled plasma quadrupole mass spectrometer. The device was controlled using ICP-MS-TOP ChemStation software (version G1834B). Before the measurements, the mother liquids, after solid phase separation, were diluted with an extra pure 2% HNO_3 solution. To calculate cerium concentration in the samples,

the calibration curve was obtained, by analysing standard solutions with cerium concentrations of 5, 20 and 100 μg L^{-1}. The detection limit was about 10^{-8} M. For each measurement by ICP-MS, the standard error was within 10%.

Analysis of solid substances

For solid phase characterisation before and after dissolution experiments, X-ray diffraction (XRD), high-resolution transmission electron microscopy (HRTEM), high energy resolution fluorescence detected X-ray absorption spectroscopy (HERFD-XAS) and pair distribution function (PDF) analysis were used.

Synchrotron-based XRD measurements were performed using the X-ray structural analysis (XSA) beamline of the Kurchatov Synchrotron Radiation Source (NRC "Kurchatov Institute", Moscow). For synchrotron-based XRD measurements, CeO_2 NP samples were placed in synthetic vacuum oil and mounted on a 20 μm nylon CryoLoop. The measurements were performed in the transmission mode, using a Rayonix SX-165 CCD detector at a wavelength of 0.80 Å. Raw 2D scattering images were integrated using the Fit2D software program. The PDF database was used for the identification of the crystalline phases. The particle size of nanocrystalline ceria was calculated using the Scherrer formula and the coefficient of anisotropy (*K*-factor) was set to 0.94. Line profiles for (111) and (200) reflections were fitted to pseudo-Voigt functions. Particle size was calculated from the full width at half-maximum (FWHM) of (111) and (200) diffraction lines, taking into account instrumental broadening. Instrumental broadening was calculated using the Caglioti formula.[33]

A microstructural evaluation was performed using a Jeol 2100F transmission electron microscope operating at an accelerating voltage of 200 kV. Electron diffraction patterns were recorded using the same instrument. To obtain data on average size and distribution from HRTEM images, the diameter of more than 200 particles was calculated.

HERFD-XAS experiments were performed using the BM20 beamline of the European Synchrotron Radiation Facility, Grenoble (France).[34] The incident energy was selected using the (111) reflection from a double crystal Si monochromator. Rejection of higher harmonics was achieved using two Rh mirrors working at an angle of 2.5 mrad relative to the incident beam. HERFD-XAS spectra were measured using an X-ray emission spectrometer[35] at a 90° horizontal scattering angle. The sample, analyser crystal and photon detector (avalanche photodiode) were arranged in a vertical Rowland geometry. The Ce HERFD-XAS spectra at the L_3 edge were obtained by recording the maximum intensity of the Ce $L\alpha_1$ emission line (4839 eV) as a function of the incident energy. The emission energy was selected using the (331) reflection of five spherically bent Ge crystal analysers (with R = 1 m) aligned at a 80.7° Bragg angle. The size of the beam at the sample was 400 μm horizontally and 80 μm vertically. A combined (incident convoluted with emitted) energy resolution of 1.2 eV was obtained, as determined by measuring the FWHM of the elastic peak. Samples for the HERFD-XAS measurements were prepared as wet pastes and sealed with single Kapton confinement (of 25 micron thickness).

X-ray total scattering measurements were performed using the beamline P02.1 of PETRA III at the Deutsches Elektronen-Synchrotron (DESY). Rapid acquisition data collection[36] was used with a Varex XRD 4343CT detector (2880 × 2880 pixels, 150 × 150 μm^2 each) and a sample-to-detector distance of 281.03 mm. The incident energy of the X-rays was 59.795 keV (λ = 0.20735 Å). Samples were loaded into 0.8 mm inner diameter glass capillaries. A LaB_6 standard was measured at room temperature for calibration of the detector geometry. Calibration, polarisation correction and azimuthal integration to 1D diffraction patterns were performed using Fit2D software.[37] Background subtraction of an empty capillary measurement and normalisation of the 1D diffraction intensities were carried out to obtain the total scattering structure function, $F(Q)$, which was Fourier transformed to obtain the PDF, $G(r)$, using PDFgetX3 within the xPDFsuite.[38,39] The range used in the Fourier transform was 0.3–23 $Å^{-1}$ for 8 nm NPs and 0.5–23 $Å^{-1}$ for 2 nm NPs. Structure refinements were performed using PDFgui and Diffpy-CMI (for use of the log-normal spherical distribution damping model).[40,41] The crystal structure of CeO_2 ($Fm\bar{3}m$) was refined to the resulting PDFs, including the lattice parameter a, isotropic atomic displacement parameters for Ce and O, a parameter to account for correlated motion δ_1, a spherical damping correction to account for average crystallite size and a scale factor. The contribution of the instrumental profile was determined by structure refinement to the LaB_6 standard: Q_{damp} = 0.02906 $Å^{-1}$.

Results

CeO_2 particle characterisation before dissolution experiments

Cerium dioxide nanoparticles were synthesised using a chemical precipitation method.[42] It is generally accepted that the solubility product constant of particles smaller than 100 nm depends substantially on particle size, and the difference is most significant when the size decreases from 10 to 1 nm.[43] Thus, the conditions for CeO_2 synthesis were designed to obtain NPs in this size range. Data from the literature for ceria NPs suggest that thermal treatment has a strong influence on biological impact.[44] Therefore, in addition to size variation, the samples were heat treated under different conditions. Special attention was paid to CeO_2 NP analysis before and after drying.

Fig. 1 and S1† show data characterising the structure of non-treated and dried CeO_2 NPs before the dissolution experiments. According to high-resolution transmission electron microscopy (HRTEM) data, aggregates of crystalline NPs were formed during chemical precipitation (Fig. S1a and b†). Particle size distributions for both samples confirmed a relatively low polydispersity, which has a close fit to a

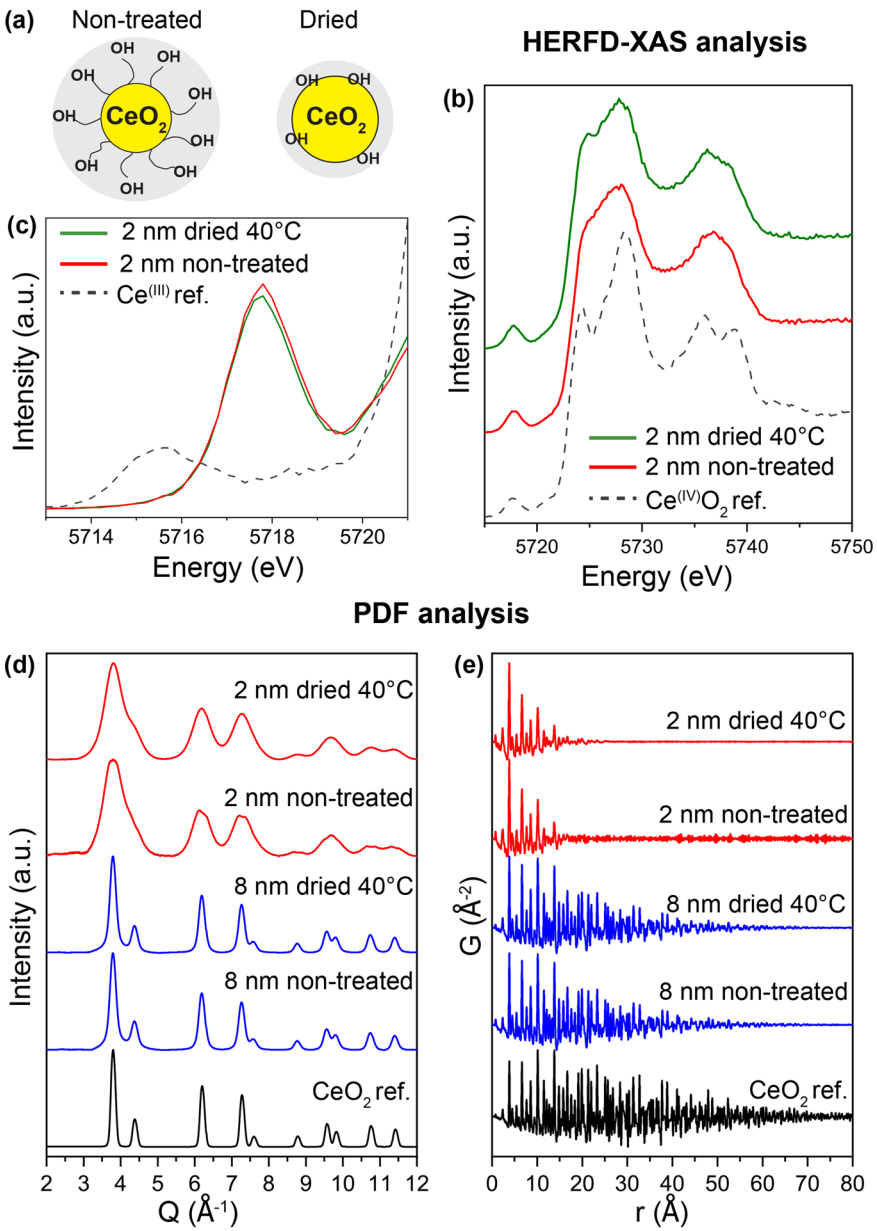

Fig. 1 (a) Schematic representation of non-treated and dried CeO_2 NPs. Non-treated CeO_2 particles obtained by chemical precipitation in solution possessed a high degree of surface hydroxylation.[42] (b) Comparison between the Ce L_3 HERFD-XAS spectra of non-treated and dried CeO_2 NPs. (c) Enlarged view of the pre-edge HERFD-XAS spectra of non-treated and dried CeO_2 NPs compared with the pre-edge spectrum of cerium(III) sulfate. (d) X-ray scattering intensity profiles of CeO_2 samples obtained by X-ray total scattering measurements. (e) The corresponding reduced pair distribution functions $G(r)$ were obtained by Fourier transformation (FT) of the data with Q_{max} = 23.0 Å^{-1}.

lognormal function (Fig. S1c and d†). According to HRTEM data, average NP diameters were 2.3 ± 0.4 nm and 7.8 ± 1.2 nm for the samples synthesised from 0.001 M and 0.8 M $Ce(NO_3)_3$, respectively. X-ray diffraction (XRD) data indicated that all the samples were single-phase and corresponded to cubic CeO_2 (PC PDF 81-792) (Fig. S2†). Crystallite sizes calculated from XRD data were 2.3 ± 0.2 nm for CeO_2 prepared from 0.001 M $Ce(NO_3)_3$ and 8.8 ± 0.9 nm for CeO_2 prepared from 0.8 M $Ce(NO_3)_3$. Diffraction data and transmission electron microscopy data obtained are in good agreement with each other, indicating that CeO_2 samples consist of single crystalline particles with no internal grain boundaries. Based on the results presented above, the samples will be referred to as "2 nm" for CeO_2 prepared from 0.001 M $Ce(NO_3)_3$ and "8 nm" for CeO_2 prepared from 0.8 M $Ce(NO_3)_3$.

Fig. 1b shows the full high energy resolution fluorescence detected X-ray absorption experimental spectra (HERFD-XAS) of CeO_2 NPs of 2 nm diameter, both non-treated and dried, compared with bulk CeO_2. Measurements were carried out at the Ce L_3 edge, which means that the electron was excited by the incident X-rays from the 2p orbital of Ce at an energy of

5723 eV. The spectra reveal the presence of dipole-allowed 2p–5d transitions (main edge transitions in the energy range 5720–5730 eV) and dipole-forbidden, but quadrupole-allowed, 2p–4f transitions (at the pre-edge in the energy range 5715–5720 eV). The main edge peaks in the L_3 HERFD-XAS spectra of 2 nm CeO_2 were essentially broader than those obtained from bulk CeO_2. This size effect in the spectra has already been discussed,[42] and is related to electron delocalisation at the surface of the 2 nm NPs, where the high surface-to-volume ratio has an impact. The effect of surface modification is clearly seen in the HERFD-XAS spectrum for 2 nm NPs dried at 40 °C and 150 °C (Fig. S4†). The spectral structure sharpened and the separation between the main edge peaks (due to the splitting of the Ce 5d states into the e_g and t_{2g} transitions in the cubic Ce crystal structure[45]) became more visible. These surface modifications may be associated with a decrease in the hydroxylation of the surface after drying.[42] In a recent study conducted by Ghosalya *et al.*[46] using the X-ray photoelectron spectroscopy method at ambient pressure it was found that hydroxyl groups were present in 2 nm and 5 nm particles. Ghosalya *et al.* observed that surface hydroxylation decreased as the temperature increased, with changes in the spectra starting at 50 °C. Thus, the results obtained in the current study are consistent with existing reports.

An enlarged view of the pre-edge spectra of non-treated and dried CeO_2 is presented in Fig. 1c. The pre-edge structure of the non-treated and dried 2 nm NPs revealed the presence of the Ce(IV) oxidation state only. The characterisation of CeO_2 NPs dried at 150 °C is presented in Fig. S3† (XRD data) and Fig. S4† (HERFD-XAS spectra). These data are in good agreement with previously reported results confirming the absence of Ce(III) in CeO_2 NPs prepared by chemical precipitation techniques and dried under various conditions.[42,46,47] Based on XRD data, it is apparent that the sizes of the CeO_2 crystallites remain unchanged upon drying of the samples (Fig. S3†). Specifically, the crystallite sizes, as determined using the Scherrer equation, are found to be 2.1 ± 0.2 nm and 2.4 ± 0.2 nm after drying at 40 °C and 150 °C, respectively. This observation indicates that the sample drying does not have any noticeable effect on the sample's crystallinity; however, the examination of HERFD-XAS suggests modifications in the surface hydroxylation caused by thermal treatment (Fig. 1a).

Pair distribution function (PDF) analysis was used to further study the local structuring of the 2 nm and 8 nm NPs before and after heat treatment.[42] Fig. 1d shows scattering intensity profiles for the samples of CeO_2 NPs investigated and a CeO_2 reference. The corresponding reduced pair distribution function $G(r)$ is shown in Fig. 1e. A model of the damping of $G(r)$ was refined in order to extract the average crystallite size: approximately 2.0 nm and 8.5 nm, respectively, in agreement with XRD and HRTEM results. In particular, the effect of crystallite size on the 2 nm samples could be better described by a lognormal spherical distribution,[48] but the mean value and width parameters of the distribution were too highly correlated to enable the provision of reliable values, in this case. Refinement of the crystal structure of CeO_2 to the local structure in the PDFs consistently resulted in a slight contraction of the lattice parameter for both NP sizes, and in an increase in the atomic displacement parameters and crystallite size for the samples dried at 40 °C (Fig. S5, Table S1†), suggesting increases in both a compressive homogeneous strain and an inhomogeneous strain.[49] It is important to note the simplicity of the models used,[50] which, in the present case, do not account for distinguishing core and surface features, but they do suggest a structural modification associated with the drying process. Since the mild temperatures used are unlikely to have had a significant impact on the CeO_2 core structure, this suggests that the removal of hydroxyl groups may lead to some surface relaxation.

To summarise the results of the dried and non-treated samples studies, the mild drying (40 °C and 150 °C) process did not affect the morphology, particle size distribution or stoichiometry of CeO_2 NPs, but it did slightly affect hydroxylation and structural strain.

CeO_2 dissolution experiments

Fig. 2a and b show the dissolution kinetics at pH = 4.1 ± 0.2 for 2 nm and 8 nm CeO_2 samples, both non-treated and dried at 40 °C and 150 °C. In each case, the time dependence of cerium concentration in the solution can be approximated by linear regression in the range of 1 to 50 days in $y = C(t)$ coordinates (Fig. S6†). Thus, the CeO_2 dissolution process could be attributed to a zero-order reaction and be independent of the concentration of initial reagents. Dissolution rate constants for CeO_2 samples are reported in Table S2.† For both 2 nm and 8 nm samples, the rate constants for non-treated samples are five times higher than those of the dried ones. This indicates the higher reactivity of the non-treated samples in comparison with the dried samples. The rate constants of dried CeO_2 samples' (40 °C and 150 °C) dissolution are very close to each other.

After 50 days of CeO_2 interaction with a solution, the concentration of dissolved cerium was virtually unchanged; thus, it might be supposed that a steady-state condition had been reached in all systems studied, at this point. The concentrations of cerium in the solution in the presence of NPs in the non-treated CeO_2 samples (2 nm and 8 nm), once the steady-state condition had been reached, were quite similar. Heat treatment did, however, lower ceria solubility by at least half an order of magnitude (Fig. 2a and b). After 160 days from the beginning of the dissolution process at pH = 4.1 ± 0.2, the cerium concentration values for the 2 nm CeO_2 NPs were 8×10^{-5} M for non-treated samples and 2×10^{-5} M for the dried samples. After the same dissolution time, for 8 nm NPs, the concentrations of cerium in the solution were 7×10^{-5} M for the non-treated sample and 2×10^{-5} M for the dried sample. Interestingly, there was no significant

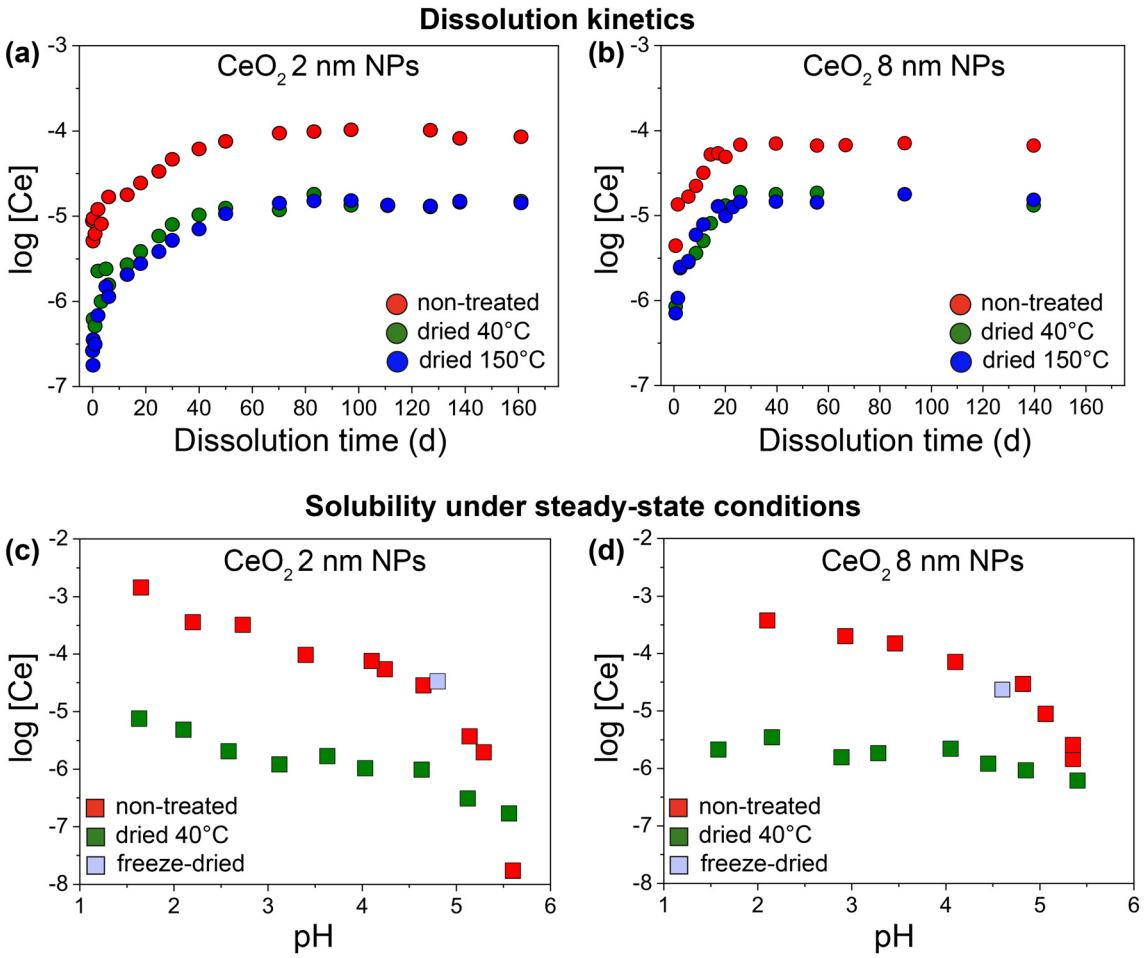

Fig. 2 (a) and (b) The kinetic curves of non-treated and dried CeO_2 samples' dissolution in 0.01 M $NaClO_4$ at pH = 4.1 ± 0.2. (c) and (d) Dependence of dissolved cerium concentration on the pH value after two months of CeO_2 solids and water media interaction.

difference in cerium concentration in the supernatant liquid between the samples dried at 40 °C and 150 °C.

Fig. 2c and d show the dependences of cerium concentration in the solution in the presence of the CeO_2 NPs under steady-state conditions, as a function of pH. The data were collected two months after the beginning of the experiment and the effect of decreasing solubility for the dried CeO_2 can be observed in a wide range of pH values. The difference in cerium concentrations for non-treated and dried samples was much more significant at low pH (pH < 4) and was nearly eliminated under neutral conditions. There was, however, still no significant difference in dissolved cerium concentration between the 2 and 8 nm CeO_2 samples (Fig. S7†).

To gain a deeper insight into the origins of the observed phenomenon, the solubility of freeze-dried CeO_2 NPs was also examined. Freeze drying is a low-temperature dehydration process that involves freezing the product and removing ice by sublimation under low pressure. This method produces samples with low aggregation and higher mesoporosity than with conventional drying.[51–53] The literature suggests a higher hydroxyl group content in freeze-dried samples than in heat-dried samples.[54] Phase stability and stoichiometry conservation during freeze-drying were confirmed by XRD and HERFD-XAS measurements (Fig. S3 and S4†). In Fig. 2c and d, the cerium concentration in solution in the presence of freeze-dried CeO_2 NPs is shown using blue squares. These values are closer to the concentration of dissolved cerium in the presence of non-treated CeO_2 at the same pH values and the trend is observed in the dissolution of both 2 and 8 nm freeze-dried NPs. Thus, the solubility behaviour of freeze-dried CeO_2 NPs resembles that of non-treated samples.

Previously, the dissolution kinetics of cerium dioxide in various media were studied in short-term experiments only – from several hours to several months.[27,28,55] The long-term behaviour (over a matter of years) of CeO_2-based nanomaterials in solutions is poorly understood. At the same time, the long-term processes could profoundly influence NPs' ecological and health risk assessments. The dependence of cerium concentration in solution on pH over different time periods is presented in Fig. 3. These data demonstrate that the dissolution of 40 °C dried CeO_2 NPs is very slow. Even after 4.5 years of solid/liquid interaction, the cerium concentration in the solution was still increasing. The concentration of cerium in solution in the presence of non-

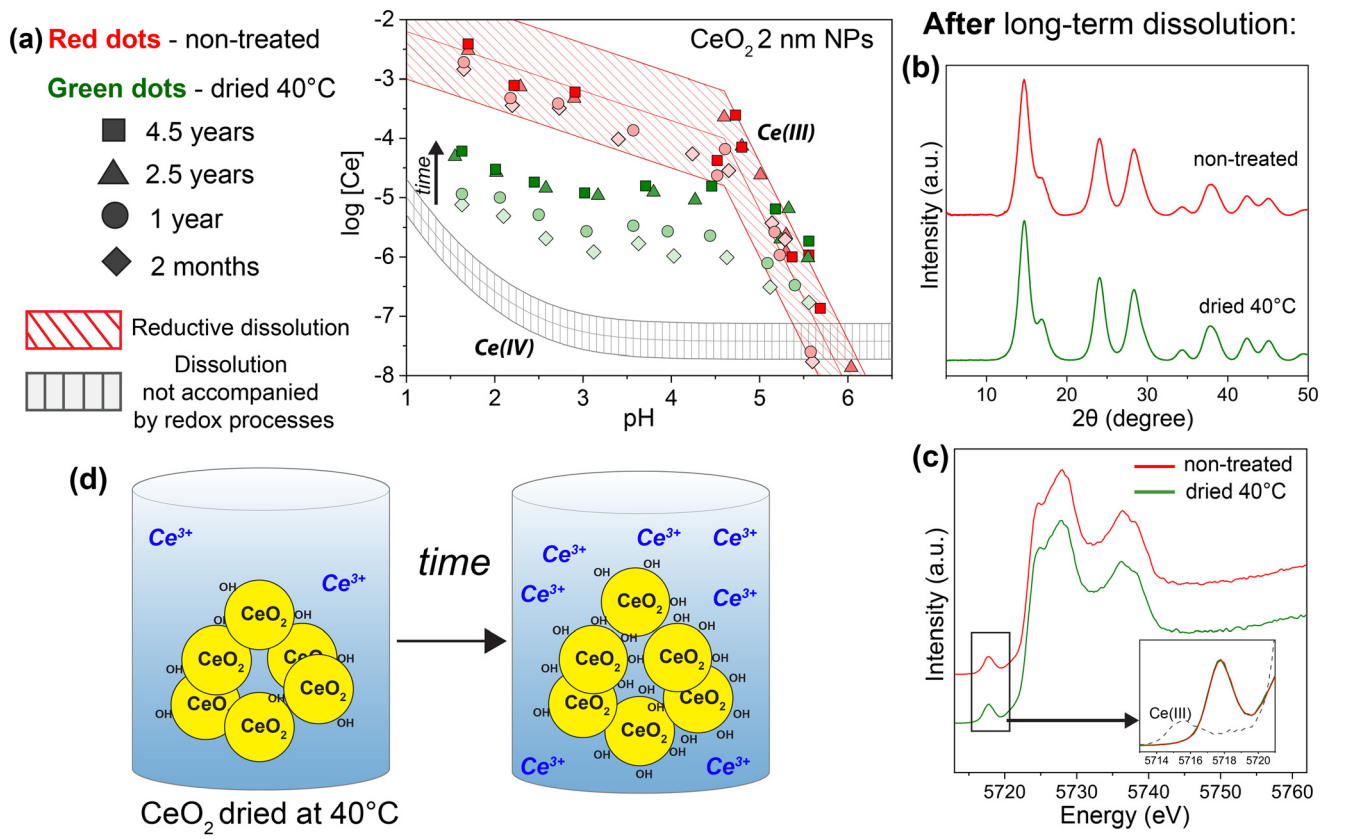

Fig. 3 (a) Cerium concentration in 0.01 M $NaClO_4$ solution in the presence of non-treated and dried CeO_2 2 nm NPs at different pH values and times of dissolution. Red hatching – the model of CeO_2 reductive solubility, calculated using $\log K_{CeO_2/Ce^{3+}} = 25.8 \pm 0.3$ and $\log K_{sp} = -59.3 \pm 0.3$ (I = 0.01).[26] Grey hatching – the model of CeO_2 solubility without redox reactions, calculated using $\log K_{sp} = -59.3 \pm 0.3$ (I = 0.01).[26] (b) Synchrotron-based XRD patterns and (c) Ce L_3 HERFD-XAS spectra of non-treated and dried CeO_2 after initial particle dissolution for 4.5 years. The inset depicts an enlarged view of the pre-edge HERFD-XAS spectra of CeO_2 samples after dissolution, along with cerium(III) sulfate. (d) Schematic representation of the dried CeO_2 dissolution mechanism based on particle dissolution and gradual hydroxylation of the particle surface.

treated CeO_2 particles did not change noticeably in the same experimental time period.

Non-treated and dried CeO_2 samples were analysed after prolonged contact with the aqueous media to determine the origins of solubility differences. XRD was used to investigate possible changes in the crystallinity of the samples (Fig. 3b and S8†). The HERFD-XAS method was applied to exclude the possibility of trivalent cerium formation in the crystalline structure of CeO_2 NPs during dissolution and to assess any changes in the degree of surface hydroxylation (Fig. 3c). HRTEM was used to further analyse the morphological features of NPs after dissolution (Fig. S7†). No significant changes in the structure and morphology of NPs after contact with the solution were revealed. This suggests that the solubility of NPs is controlled only by the subtle changes occurring with the particles during drying. These differences and the possible mechanism of dissolution of non-treated and dried particles are described in the "Discussion" section.

A thermodynamic description of the dissolution process is necessary for calculating the solubility product constant (K_{sp}). There is a hypothesis in the literature that, in the case of incomplete separation of the solid phase and the solution, so-called eigencolloids within the size range of 1.5–2 nm may remain in the solution.[56–58] In particular, Neck *et al.* revealed such phenomena while studying the solubility of thorium and plutonium dioxides.[57,58] When no, or insufficient, phase separation occurs, the measured Th(IV) and Pu(IV) concentrations in the aqueous phase are generally ~2.5 orders of magnitude larger. Thus, many studies have proposed the use of ultrafiltration or ultracentrifugation to calculate the K_{sp} of dissolved actinide oxides to minimise the influence of eigencolloids on the value of the constant.

Because CeO_2 eigencolloids could influence the experimental results, different ways of separating NPs from the solution were used in the present study. Generally, high-speed long-term centrifugation was used for solid separation from the solution. In several cases, ultracentrifugation was also used, to rule out experimental error and the possible incomplete separation of CeO_2 NPs. The results obtained showed no differences in the concentration of dissolved cerium after different types of centrifugation of the same sample (Table S3†). Thus, the CeO_2 NP solubility product constant could be calculated from the experimental results.

The dissolution of cerium dioxide under pH < 7 is accompanied by the formation of Ce(III) aqueous species. Thus, CeO_2 solubility data could be fitted based on the

reductive dissolution thermodynamical model.[26] The concentration of dissolved cerium, in the case of the dissolution of the 40 °C dried CeO_2 sample, constantly increased under a pH of 1.5–6; the system was far from a thermodynamic equilibrium (Fig. 3a). Therefore, calculating the solubility product constant from these experimental data may be erroneous. The cerium concentration in solution for non-treated CeO_2 samples remained practically unchanged for 4.5 years. This suggests that the non-treated CeO_2 NPs/water system was closer to the thermodynamic equilibrium than the dried CeO_2 NPs/water system, so the solubility constant could be estimated based on experimental data for non-treated CeO_2. The solubility product constant for non-treated CeO_2 was $\log K_{sp} = -59.3 \pm 0.3$ at ionic strength 0.01 M.

Discussion

Summarising the experimental results, the following abnormalities in the solubility behaviour of CeO_2 should be highlighted. Unexpectedly, the solubility of CeO_2 NPs did not noticeably depend on particle size, in the range of 2–8 nm, while the solubility of non-treated samples was much higher than that of the dried ones. The differences in the solubility of dried, and non-treated, CeO_2 nanoparticles decreased significantly when the pH of the media increased from 1.5 to 6. There was no apparent difference in the solubility of NPs dried at 40 °C and 150 °C. The prolonged storage (up to 4.5 years) of CeO_2 NPs in aqueous media caused the dissolution of dried samples to gradually increase, while for non-treated samples, it remained virtually unchanged. The phase structure, morphology and cerium oxidation state in NPs remaining in solution were preserved during long-term dissolution in the case of both non-treated and dried CeO_2.

It is generally accepted that the solubility of a particle increases as size decreases. This phenomenon results from the increased chemical potential found at curved surfaces,[59] which is the basis for particle growth, according to Ostwald ripening.[11] Apparently, this is not an applicable description for the CeO_2 NPs studied here, and possibly, nor is it for other less soluble particles. Next, there will be a discussion of the process of dissolution of CeO_2, with an attempt to explain the observed abnormal experimental observations.

The solubility of CeO_2 is controlled by a few monolayers on the surface, which cannot be properly probed by any of the sophisticated techniques considered in this work. This hypothesis is in line with previous studies that have revealed that the dissolution process of cerium dioxide and other less soluble substances is not representative of the bulk phase, but is rather controlled by the surface processes of a few monolayers of the corresponding oxide.[28,29,60–62] After chemical precipitation, a significant amount of hydroxyl groups is present on the surface of CeO_2 particles. Some studies have proposed considering particles of metal dioxides obtained from solutions as being particles with a core/shell structure, or even proposed judging the hydroxylated surface layer as a microphase.[63] The surface of hydrated NPs is not a simple, planar, sharp boundary, but is better thought of as a perturbed boundary region.[16] When particles are extremely small, such perturbed regions are dominant and the notions of "phase" and "surface" become ambiguous. Any drying processes should lead to a decrease in the degree of hydroxylation.[42] Therefore, the complex surface layer of 2 and 8 nm CeO_2 particles originating from the synthesis and post-synthesis treatment could control solubility and be the reason for the solubility of particles of different sizes being the same.

Since the dissolution of cerium dioxide occurs by the mechanism of reductive dissolution, the surface state plays a vital role. The reductive dissolution of cerium dioxide occurs due to the interaction of surface Ce(IV) ions and a partially negative electronic charge on water oxygen.[26] According to HERFD-XAS (Fig. 1b), even a mild drying, at 40 °C, leads to modification of the particle surface, which is most likely associated with the removal of hydroxyl groups during drying.[42] According to local structure refinements for non-treated and dried CeO_2 NPs of various sizes, consistent changes in cell parameters and displacement parameters upon the drying of 2 nm and 8 nm NPs also suggest some structural modifications (Table S1†). These modifications are likely to be driven by changes in the surface environment of NPs due to decreased hydroxylation. Consequently, the affinity to water oxygen atoms of the dried surface may decrease, so reducing the potential of the cerium reduction reaction. Thus, the solubility of the dried CeO_2 particles decreases in comparison with that of the non-treated samples. This hypothesis was confirmed indirectly by the fact that the solubility of freeze-dried samples was quite close to the solubility of non-treated particles (Fig. 2), because freeze-drying preserves the original surface properties.

Further confirmation of surface-derived CeO_2 dissolution is provided by the pronounced difference in the solubility of the non-treated and dried particles under different pH values. The thermodynamic stability of Ce(III) in solution is the driving force behind reductive dissolution. At the same time, the influence of Ce(III) on the dissolution of CeO_2 weakens with increasing pH.[25] A decrease in the dissolved cerium concentration difference in the case of the dissolution of dried and non-treated samples, with an increase in pH, was also observed.

Last but not least is the question that arises from the analysis of experimental data as to why the dissolution of dried particles constantly increases for 4.5 years and tends to the values of non-treated samples. According to existing literature data for some oxides, surface energy depends not only on particle size, but also on morphology, dopants, surface hydroxylation, *etc.*[15,16,64,65] Hydration lowers surface energy by 20–30%.[16] Such an effect has been observed only at the nanoscale and has been reported for Al_2O_3, Fe_2O_3, TiO_2, SnO_2, UO_2 and other systems.[14–18,65] Thus, the dried surface should have the highest surface enthalpy and relax its high-energy surface sites by water adsorption. Over time, water

molecules may dissociate on the surface of the dried particles to repair incomplete bonding geometries on the initial surface. Thus, the surface of the dried CeO_2 tends to return to its original highly-hydrated and more energetically favourable state (Fig. 3d). All these factors affect one of the most essential CeO_2 macro properties – the solubility of the particles.

We hypothesize that the effect of surface hydroxylation could also be observed in other low soluble compounds. Here, one possible example could be PuO_2, with the crystal structure beign similar to that of CeO_2. Although the effect of drying on dissolution has not been studied yet for PuO_2, it should be noted that this compound tends to form fluorite-type crystalline nanoparticles and the solubility product constants of CeO_2 and PuO_2 are quite close.[66–68] Furthermore, the influence of surface hydroxylation on dissolution behaviour was observed earlier for HfO_2 and MgO.[69,70] The solubility of metal hydroxides or X-ray amorphous oxides, such as $Zr(OH)_4$ or ThO_2(am), has been shown to decrease after thermal treatment due to the crystallization during ageing or drying.[71–74] Based on our findings, it is also reasonable to consider surface hydroxylation when describing the solubility mechanism in nanocrystalline systems of ZrO_2 and ThO_2.

Conclusions

The hydrated surface of cerium dioxide is an important feature that determines CeO_2 particles' properties, including solubility. Non-treated CeO_2 nanoparticles exhibit a much higher solubility than dried ones, across a wide pH range (pH 1.5–6), suggesting that the hydroxylated surface catalyses dissolution processes. Meanwhile, the dissolution of dried CeO_2 gradually increases with time, on the evidence of a 4.5 year observation period. This probably happens because water dissociates on the dried CeO_2 particle surface, to complete bonding geometries and return it to the hydrated state. Comparison of the experimental and literature data leads to the conclusion that the hydrated surface significantly reduces surface energy at the nanoscale, which ensures the stabilisation of NPs for a long time. Particles' stability and solubility play a crucial role in their bioactivity (biopersistence, toxicity, *etc.*) and, of course, in the key technological processes (*e.g.*, in catalysis). Therefore, the NPs' surface hydroxylation and their stability should be considered in all fields associated with nanomaterial application and regulation.

Abbreviations

NPs	Nanoparticles
XRD	X-ray diffraction
HRTEM	High-resolution transmission electron microscopy
HERFD-XAS	High energy resolution fluorescence detected X-ray absorption spectroscopy
PDF	Pair distribution function

Author contributions

T. V. P., A. Yu. R. and A. D. K. conceived, designed and performed the experiments. I. F. S. performed ICP-MS measurements. A. E. B. performed the cryo experiments and lab-XRD measurements. R. D. S. and M. W. T. performed PXRD measurements and processed the results. T. V. P., A. Yu. R., M. W. T., A. E. B., V. K. I. and S. N. K. discussed the results and co-wrote the paper.

Conflicts of interest

The authors declare no competing interests.

Acknowledgements

The study was supported by the Russian Science Foundation (grant no. 23-73-30006). We acknowledge ESRF for beamtime allocation for proposal MD-1213 and Dr Kristina Kvashnina and Dr Elena Bazarkina for their help with Ce L_3-edge HERFD-XANES measurements. We thank the ID26 beamline of ESRF for providing the Ge crystal. The authors also thank Dr Kristina Kvashnina for valuable data discussions and manuscript editing. We acknowledge DESY (Hamburg, Germany), a member of the Helmholtz Association HGF, for the provision of experimental facilities. Parts of this research were carried out at PETRA III and we would like to thank Martin Etter for assistance in using beamline P02.1. Beamtime was allocated for proposal RAt-20010283.

References

1 H. Pahlevaninezhad, M. Khorasaninejad, Y. W. Huang, Z. Shi, L. P. Hariri, D. C. Adams, V. Ding, A. Zhu, C. W. Qiu, F. Capasso and M. J. Suter, Nano-optic endoscope for high-resolution optical coherence tomography in vivo, *Nat. Photonics*, 2018, **12**, 540–547.
2 D. Deng, K. S. Novoselov, Q. Fu, N. Zheng, Z. Tian and X. Bao, Catalysis with two-dimensional materials and their heterostructures, *Nat. Nanotechnol.*, 2016, **11**, 218–230.
3 S. Mann, Self-assembly and transformation of hybrid nano-objects and nanostructures under equilibrium and non-equilibrium conditions, *Nat. Mater.*, 2009, **8**, 781–792.
4 M. L. Juan, M. Righini and R. Quidant, Plasmon nano-optical tweezers, *Nat. Photonics*, 2011, **5**, 349–356.
5 P. Cervantes-Avilés, X. Huang and A. A. Keller, Dissolution and Aggregation of Metal Oxide Nanoparticles in Root Exudates and Soil Leachate: Implications for Nanoagrochemical Application, *Environ. Sci. Technol.*, 2021, **55**, 13443–13451.
6 J. Hou, H. Liu, L. Wang, L. Duan, S. Li and X. Wang, Molecular Toxicity of Metal Oxide Nanoparticles in Danio rerio, *Environ. Sci. Technol.*, 2018, **52**, 7996–8004.
7 R. M. Molina, N. V. Konduru, R. J. Jimenez, G. Pyrgiotakis, P. Demokritou, W. Wohlleben and J. D. Brain, Bioavailability, distribution and clearance of tracheally instilled, gavaged or

injected cerium dioxide nanoparticles and ionic cerium, *Environ. Sci.: Nano*, 2014, **1**, 561–573.
8 L. Goswami, K. H. Kim, A. Deep, P. Das, S. S. Bhattacharya, S. Kumar and A. A. Adelodun, Engineered nano particles: Nature, behavior, and effect on the environment, *J. Environ. Manage.*, 2017, **196**, 297–315.
9 C. Walther and M. A. Denecke, Actinide colloids and particles of environmental concern, *Chem. Rev.*, 2013, **113**, 995–1015.
10 T. Xia, M. Kovochich, M. Liong, L. Mädler, B. Gilbert, H. Shi, J. I. Yeh, J. I. Zink and A. E. Nel, Comparison of the mechanism of toxicity of zinc oxide and cerium oxide nanoparticles based on dissolution and oxidative stress properties, *ACS Nano*, 2008, **2**, 2121–2134.
11 P. W. Voorhees, The Theory of Ostwald Ripening, *J. Stat. Phys.*, 1985, **38**, 231–252.
12 A. Navrotsky, Progress and new directions in high temperature calorimetry revisited, *Phys. Chem. Miner.*, 1997, **24**, 222–241.
13 L. Vayssieres, On the thermodynamic stability of metal oxide nanoparticles in aqueous solutions, *Int. J. Nanotechnol.*, 2005, **2**, 411–439.
14 X. Guo, D. Wu, S. V. Ushakov, T. Shvareva, H. Xu and A. Navrotsky, Energetics of hydration on uranium oxide and peroxide surfaces, *J. Mater. Res.*, 2019, **34**, 3319–3325.
15 N. Birkner and A. Navrotsky, Thermodynamics of manganese oxides: Effects of particle size and hydration on oxidation-reduction equilibria among hausmannite, bixbyite, and pyrolusite, *Am. Mineral.*, 2012, **97**, 1291–1298.
16 A. Navrotsky, Nanoscale effects on thermodynamics and phase equilibria in oxide systems, *ChemPhysChem*, 2011, **12**, 2207–2215.
17 J. M. McHale, A. Auroux, A. J. Perrotta and A. Navrotsky, Surface energies and thermodynamic phase stability in nanocrystalline aluminas, *Science*, 1997, **277**, 788–789.
18 A. Navrotsky, L. Mazeina and J. Majzlan, Size-driven structural and thermodynamic complexity in iron oxides, *Science*, 2008, **319**, 1635–1638.
19 S. N. Kalmykov and M. A. Denecke, *Actinide Nanoparticle Research*, Springer, Berlin, Heidelberg, 2011.
20 Y. Li, X. Hou, C. Yang, Y. Pang, X. Li, G. Jiang and Y. Liu, Photoprotection of Cerium Oxide Nanoparticles against UVA radiation-induced Senescence of Human Skin Fibroblasts due to their Antioxidant Properties, *Sci. Rep.*, 2019, **9**, 2595.
21 N. Daelman, M. Capdevila-Cortada and N. López, Dynamic charge and oxidation state of Pt/CeO_2 single-atom catalysts, *Nat. Mater.*, 2019, **18**, 1215–1221.
22 E. Casals, M. Zeng, M. Parra-Robert, G. Fernández-Varo, M. Morales-Ruiz, W. Jiménez, V. Puntes and G. Casals, Cerium Oxide Nanoparticles: Advances in Biodistribution, Toxicity, and Preclinical Exploration, *Small*, 2020, **16**, 1–22.
23 C. K. Kim, T. Kim, I. Y. Choi, M. Soh, D. Kim, Y. J. Kim, H. Jang, H. S. Yang, J. Y. Kim, H. K. Park, S. P. Park, S. Park, T. Yu, B. W. Yoon, S. H. Lee and T. Hyeon, Ceria Nanoparticles that can Protect against Ischemic Stroke, *Angew. Chem., Int. Ed.*, 2012, **51**, 11039–11043.
24 Z. Li, D. Piankova, Y. Yang, Y. Kumagai, H. Zschiesche, M. Jonsson, N. V. Tarakina and I. L. Soroka, Radiation Chemistry Provides Nanoscopic Insights into the Role of Intermediate Phases in CeO_2 Mesocrystal Formation, *Angew. Chem., Int. Ed.*, 2022, **61**, e202112204.
25 S. A. Hayes, P. Yu, T. J. O'Keefe, M. J. O'Keefe and J. O. Stoffer, The Phase Stability of Cerium Species in Aqueous Systems, *J. Electrochem. Soc.*, 2002, **149**, C623.
26 T. V. Plakhova, A. Y. Romanchuk, S. N. Yakunin, T. Dumas, S. Demir, S. Wang, S. G. Minasian, D. K. Shuh, T. Tyliszczak, A. A. Shiryaev, A. V. Egorov, V. K. Ivanov and S. N. Kalmykov, Solubility of Nanocrystalline Cerium Dioxide: Experimental Data and Thermodynamic Modeling, *J. Phys. Chem. C*, 2016, **120**, 22615–22626.
27 J. T. Dahle, K. Livi and Y. Arai, Effects of pH and phosphate on CeO_2 nanoparticle dissolution, *Chemosphere*, 2015, **119**, 1365–1371.
28 E. A. Grulke, M. J. Beck, R. A. Yokel, J. M. Unrine, U. M. Graham and M. L. Hancock, Surface-controlled dissolution rates: A case study of nanoceria in carboxylic acid solutions, *Environ. Sci.: Nano*, 2019, **6**, 1478–1492.
29 R. A. Yokel, M. L. Hancock, E. A. Grulke, J. M. Unrine, A. K. Dozier and U. M. Graham, Carboxylic acids accelerate acidic environment-mediated nanoceria dissolution, *Nanotoxicology*, 2019, 1–21.
30 G. Cornelis, B. Ryan, M. J. McLaughlin, J. K. Kirby, D. Beak and D. Chittleborough, Solubility and batch retention of CeO_2 nanoparticles in soils, *Environ. Sci. Technol.*, 2011, **45**, 2777–2782.
31 I. Romer, S. M. Briffa, Y. A. R. Dasilva, D. Hapiuk, V. Trouillet, R. E. Palmer and E. Valsami-Jones, Impact of particle size, oxidation state and capping agent of different cerium dioxide nanoparticles on the phosphate-induced transformations at different pH and concentration, *PLoS One*, 2019, **14**, 1–17.
32 F. Schwabe, R. Schulin, P. Rupper, A. Rotzetter, W. Stark and B. Nowack, Dissolution and transformation of cerium oxide nanoparticles in plant growth media, *J. Nanopart. Res.*, 2014, **16**, 2668.
33 G. Caglioti, A. Paoletti and F. P. Ricci, Choice of Collimators for a Crystal Spectrometer for Neutron Diffraction, *Nucl. Instrum.*, 1958, **3**, 223–228.
34 A. C. Scheinost, J. Claussner, J. Exner, M. Feig, S. Findeisen, C. Hennig, K. O. Kvashnina, D. Naudet, D. Prieur, A. Rossberg, M. Schmidt, C. Qiu, P. Colomp, C. Cohen, E. Dettona, V. Dyadkin and T. Stumpf, ROBL-II at ESRF: A synchrotron toolbox for actinide research, *J. Synchrotron Radiat.*, 2021, **28**, 333–349.
35 K. O. Kvashnina and A. C. Scheinost, A Johann-type X-ray emission spectrometer at the Rossendorf beamline, *J. Synchrotron Radiat.*, 2016, **23**, 836–841.
36 P. J. Chupas, X. Qiu, J. C. Hanson, P. L. Lee, C. P. Grey and J. L. Billinge, Rapid-acquisition pair distribution function (RA-PDF) analysis, *J. Appl. Crystallogr.*, 2003, **36**, 1342–1347.

37 A. P. Hammersley, FIT2D: A multi-purpose data reduction, analysis and visualization program, *J. Appl. Crystallogr.*, 2016, **49**, 646–652.
38 P. Juhás, T. Davis, C. L. Farrow and S. J. L. Billinge, PDFgetX3: A rapid and highly automatable program for processing powder diffraction data into total scattering pair distribution functions, *J. Appl. Crystallogr.*, 2013, **46**, 560–566.
39 X. Yang, P. Juhas, C. L. Farrow and S. J. L. Billinge, xPDFsuite: an end-to-end software solution for high throughput pair distribution function transformation, visualization and analysis, *J. Appl. Crystallogr.*, 2014, 1–4.
40 C. L. Farrow, P. Juhas, J. W. Liu, D. Bryndin, E. S. Boin, J. Bloch, T. Proffen and S. J. L. Billinge, PDFfit2 and PDFgui: Computer programs for studying nanostructure in crystals, *J. Phys.: Condens.Matter*, 2007, **19**, 335219.
41 P. Juhás, C. L. Farrow, X. Yang, K. R. Knox and S. J. L. Billinge, Complex modeling: A strategy and software program for combining multiple information sources to solve ill posed structure and nanostructure inverse problems, *Acta Crystallogr., Sect. A: Found. Adv.*, 2015, **71**, 562–568.
42 T. V. Plakhova, A. Y. Romanchuk, S. M. Butorin, A. D. Konyukhova, A. V. Egorov, A. A. Shiryaev, A. E. Baranchikov, P. V. Dorovatovskii, T. Huthwelker, E. Gerber, S. Bauters, M. M. Sozarukova, A. C. Scheinost, V. K. Ivanov, S. N. Kalmykov and K. O. Kvashnina, Towards the surface hydroxyl species in CeO_2 nanoparticles, *Nanoscale*, 2019, **11**, 18142–18149.
43 W. Wu and G. H. Nancollas, A new understanding of the relationship between solubility and particle size, *J. Solution Chem.*, 1998, **27**, 521–531.
44 A. S. Karakoti, P. Munusamy, K. Hostetler, V. Kodali, S. Kuchibhatla, G. Orr, J. G. Pounds, J. G. Teeguarden, B. D. Thrall and D. R. Baer, Preparation and characterization challenges to understanding environmental and biological impacts of ceria nanoparticles, *Surf. Interface Anal.*, 2012, **44**, 882–889.
45 D. Prieur, W. Bonani, K. Popa, O. Walter, K. W. Kriegsman, M. H. Engelhard, X. Guo, R. Eloirdi, T. Gouder, A. Beck, T. Vitova, A. C. Scheinost, K. Kvashnina and P. Martin, Size Dependence of Lattice Parameter and Electronic Structure in CeO_2 Nanoparticles, *Inorg. Chem.*, 2020, **59**, 5760–5767.
46 M. K. Ghosalya, X. Li, A. Beck, J. A. Van Bokhoven and L. Artiglia, Size of ceria particles influences surface hydroxylation and hydroxyl stability, *J. Phys. Chem. C*, 2021, **125**, 9303–9309.
47 J.-D. Cafun, K. O. Kvashnina, E. Casals, V. F. Puntes and P. Glatzel, Absence of Ce^{3+} Sites in Chemically Active Colloidal Ceria Nanoparticles, *ACS Nano*, 2013, **7**, 10726–10732.
48 L. Gamez-Mendoza, M. W. Terban, S. J. L. Billinge and M. Martinez-Inesta, Modelling and validation of particle size distributions of supported nanoparticles using the pair distribution function technique, *J. Appl. Crystallogr.*, 2017, **50**, 741–748.
49 X. Yang, A. S. Masadeh, J. R. McBride, E. S. Božin, S. J. Rosenthal and S. J. L. Billinge, Confirmation of disordered structure of ultrasmall CdSe nanoparticles from X-ray atomic pair distribution function analysis, *Phys. Chem. Chem. Phys.*, 2013, **15**, 8480–8486.
50 S. Banerjee, C. H. Liu, J. D. Lee, A. Kovyakh, V. Grasmik, O. Prymak, C. Koenigsmann, H. Liu, L. Wang, A. M. M. Abeykoon, S. S. Wong, M. Epple, C. B. Murray and S. J. L. Billinge, Improved Models for Metallic Nanoparticle Cores from Atomic Pair Distribution Function (PDF) Analysis, *J. Phys. Chem. C*, 2018, **122**, 29498–29506.
51 O. A. Shlyakhtin and Y. J. Oh, Inorganic cryogels for energy saving and conversion, *J. Electroceram.*, 2009, **23**, 452–461.
52 W. Abdelwahed, G. Degobert, S. Stainmesse and H. Fessi, Freeze-drying of nanoparticles: Formulation, process and storage considerations, *Adv. Drug Delivery Rev.*, 2006, **58**, 1688–1713.
53 G. Chen and W. Wang, Role of freeze drying in nanotechnology, *Drying Technol.*, 2007, **25**, 29–35.
54 M. Jafarzadeh, I. A. Rahman and C. S. Sipaut, Synthesis of silica nanoparticles by modified sol-gel process: The effect of mixing modes of the reactants and drying techniques, *J. Sol-Gel Sci. Technol.*, 2009, **50**, 328–336.
55 Y. Ziouane, T. Milhau, M. Maubert, B. Arab-Chapelet and G. Leturcq, Dissolution kinetics of CeO_2 powders with different morphologies and analogy to PuO_2 dissolution, *Hydrometallurgy*, 2018, **177**, 205–213.
56 M. Altmaier, V. Neck and Th. Fanghänel, Solubility and colloid formation of Th(IV) in concentrated NaCl and $MgCl_2$ solution, *Radiochim. Acta*, 2004, **92**, 537–543.
57 V. Neck, M. Altmaier and T. Fanghänel, Thermodynamic data for hydrous and anhydrous $PuO_{2+x}(s)$, *J. Alloys Compd.*, 2007, **444–445**, 464–469.
58 T. Fanghänel and V. Neck, Aquatic chemistry and solubility phenomena of actinide oxides/hydroxides, *Pure Appl. Chem.*, 2002, **74**, 1895–1907.
59 C. A. Johnson, Generalization of the Gibbs-Thomson equation, *Surf. Sci.*, 1965, **3**, 429–444.
60 J. Vandenborre, B. Grambow and A. Abdelouas, Discrepancies in thorium oxide solubility values: Study of attachment/detachment processes at the solid/solution interface, *Inorg. Chem.*, 2010, **49**, 8736–8748.
61 K. M. Peruski and B. A. Powell, Effect of calcination temperature on neptunium dioxide microstructure and dissolution, *Environ. Sci.: Nano*, 2020, **7**, 3869–3876.
62 C. Kiefer, T. Neill, N. Cevirim-Papaioannou, D. Schild, X. Gaona, T. Vitova, K. Dardenne, J. Rothe, M. Altmaier and H. Geckeis, Interlink between solubility, structure, surface and thermodynamics in the $ThO_{2(s,hyd)}$–$H_2O(l)$ system, *Front. Chem.*, 2022, **10**, 1042709.
63 C. Micheau, M. Virot, S. Dourdain, T. Dumas, D. Menut, P. L. Solari, L. Venault, O. Diat, P. Moisy and S. I. Nikitenko, Relevance of formation conditions to the size, morphology and local structure of intrinsic plutonium colloids, *Environ. Sci.: Nano*, 2020, **7**, 2252–2266.

64 R. H. R. Castro and B. Wang, The hidden effect of interface energies in the polymorphic stability of nanocrystalline titanium dioxide, *J. Am. Ceram. Soc.*, 2011, **94**, 918–924.
65 C. H. Chang, M. Gong, S. Dey, F. Liu and R. H. R. Castro, Thermodynamic stability of SnO_2 nanoparticles: The role of interface energies and dopants, *J. Phys. Chem. C*, 2015, **119**, 6389–6397.
66 A. Y. Romanchuk, T. V. Plakhova, A. V. Egorov, T. B. Egorova, P. V. Dorovatovskii, Y. V. Zubavichus, A. A. Shiryaev and S. N. Kalmykov, Redox-mediated formation of plutonium oxide nanoparticles, *Dalton Trans.*, 2018, **47**, 11239–11244.
67 E. Gerber, A. Yu. Romanchuk, I. Pidchenko, L. Amidani, A. Rossberg, C. Hennig, G. B. M. Vaughan, A. Trigub, T. Egorova, S. Bauters, T. Plakhova, M. O. J. Y. Hunault, S. Weiss, S. M. Butorin, A. C. Scheinost, S. N. Kalmykov and K. O. Kvashnina, The missing pieces of the PuO_2 nanoparticle puzzle, *Nanoscale*, 2020, **12**, 18039–18048.
68 R. J. Lemire, J. Fuger, K. Spahiu, J. C. Sullivan, H. Nitsche, W. J. Ullman, P. Potter, P. Vitorge, M. H. Rand, H. Wanner and J. Rydberg, *NEA, Chemical Thermodynamics of Neptunium and Plutonium*, OECD Publishing, Paris, 2001.
69 D. Rai, A. Kitamura, K. M. Rosso, T. Sasaki and T. Kobayashi, Issues concerning the determination of solubility products of sparingly soluble crystalline solids: Solubility of HfO_2(cr), *Radiochim. Acta*, 2016, **104**, 583–592.
70 R. A. Wogeliljs, K. Refson, D. G. Fraser, G. W. Grime and J. P. Goff, Periclase surface hydroxylation during dissolution, *Geochim. Cosmochim. Acta*, 1995, **59**, 1875–1881.
71 T. Kobayashi, T. Sasaki, I. Takagi and H. Moriyama, Effect of solid phase transformation on the solubility product of thorium hydrous oxide at 363 K, *J. Nucl. Sci. Technol.*, 2016, **53**, 1787–1793.
72 T. Kobayashi, T. Sasaki, I. Takagi and H. Moriyama, Solubility of Zirconium(IV) Hydrous Oxides, *J. Nucl. Sci. Technol.*, 2007, **44**, 90–94.
73 S. Nishikawa, T. Kobayashi, T. Sasaki and I. Takagi, Solubilities and solubility products of thorium hydroxide under moderate temperature conditions, *Radiochim. Acta*, 2018, **106**, 655–667.
74 T. Kobayashi, D. Bach, M. Altmaier, T. Sasaki and H. Moriyama, Effect of temperature on the solubility and solid phase stability of zirconium hydroxide, *Radiochim. Acta*, 2013, **101**, 645–651.

